Theoretical and Experimental Investigation of Transient Temperature Distribution in Friction Stir Welding of AA 7020-T53

Dr. Muhsin Jaber Jweeg
Nahrain University/College of Engineering
Mechanical engineering department
muhsinnah_eng@nahrainuniv.edu.iq

Dr. Moneer Hameed Tolephih
Foundation of technical education
Technical College-Baghdad
monerht@yahoo.com

Muhammed Abdul-Sattar
Nahrain University/College of Engineering
Mechanical engineering department
m1976sjn@yahoo.com

Abstract:

Finite element modeling of transient temperature distribution is used to understand physical phenomena occurring during the dwell (penetration) phase and moving of welding tool in friction stir welding (FSW) of 5mm plate made of 7020-T53 aluminum alloy at 1400rpm and 40mm/min.

Thermocouples are used in locations near to the pin and under shoulder surface to study the welding tool penetration in the workpiece in advance and retreate sides along welding line in three positions (penetrate (start welding) , mid, pullout (end welding)).

Numerical results of ANSYS 12.0 package are compared to experimental data including axial load measurements at different tool rotational speeds (710rpm.900rpm.1120rpm and 1400rpm) Based on the experimental records of transient temperature at several specific locations of thermocouples during the friction stir welding process the temperatures are higher on the advancing side (629.2 ^{o}K) than the retreating side (605 ^{o}K) along welding line and temperature in the top of workpiece under tool shoulder is higher(645 ^{o}K) than bottom (635.79^{o}K). The results of the simulation are in good agreement with that of experimental results. The peak temperature obtained was 70% of the melting point of parent metal.

الخلاصة

موديل رياضي بطريقة العناصر المحددة استخدم لتمثيل التوزيع الحراري العابروفهم الظواهر الفيزياوية التي تحدث اثناء عملية الغرز (دخول) و حركة اداة اللحام في عملية اللحام بطريقة اللخلط الاحتكا ك لصفيحة من سبيكة الالمنيوم (7020-T53) بسمك 5 ملم عند(سرعة دورانية 1400rpm , سرعة خطية40mm/min). النتائج النظرية باستخدام (ANSYS 12.0)قورنت مع النتائج العملية متضمنة قياس الحمل العمودي عمليا لعدة سرع دورانية (710rpm،900rpm, 1120rpm،1400rpm)

في هذا العمل تم استخدام مزدوجات حرارية وضعت في مواقع قريبة من راس اداة اللحام (pin) وتحت (shoulder) لغرض دراسة عملية دخول وكيفية توزيع الحرارة على جانبي وتحت اداة اللحام و لثلاث مناطق من الصفيحة (منطقة الغرز ،وسط، نهاية اللحام (خروج اداة اللحام)).

بالاعتماد على النتائج العملية المسجلة للتوزيع الحراري العابر عند مواقع مختلفة للمزدوجات الحرارية على جانبي اداة اللحام خلال عملية اللحام الخلط الاحتكاك وجد ان درجة الحرارة في منطقة (629.2 ^{o}K advance) هي اعلى من منطقة (605 ^{o}K retreate) على طول خط اللحام كما ان الحرارة عند سطح العينة تحت (645 ^{o}K shoulder) هي اعلى من اسفل العينة (635.79^{o}K)،اقصى حرارة سجلت كانت 70% من درجة الانصهار للسبيكة الامنيوم .نتائج الموديل الرياضي كانت متوافقة مع النتائج العملية .

Keywords Friction stir welding, Transient temperature, Temperature distribution, FE-simulation, 7020-T53 Aluminum alloy.

Introduction:

Friction stir welding (FSW) is a relatively contemporary solid-state process introduced back in 1991 by TWI [1]. Based on its advantages, this welding procedure has become more popular recently. Some of these advantages include however, not limited to the following: low shrinkage and distortion, desired mechanical properties, producing less fumes, and ability in welding of alloys otherwise difficult with other melting procedures, alloys such as 2xxx and 7xxx series of aluminum [2]. It could safely be stated that most if not all abovementioned advantages are due to the fact that the generated heat produced by the process remains below melting temperature of the metal. Consequently, undesired parameters resulted from typical welding processes will not materialize. Some of these parameters are solidification cracking, liquidation cracking, and porosity.

Friction stir welding fundamental is depicted in Fig. 1. In this procedure, two plates are firmly clamped on the backing plate. Spinning tool slowly lowers into the connecting plates until tool shoulder touches the upper surfaces of the plates. While spinning, the moving displaces forward on the piece and this causes heat due to the friction between them. The tool starts to move after pausing for warm-up of the plates. While forward moving, the tool forges the materials by spinning and as result, a strong connection will take place between the plates. In some cases, in order to provide more effective forge due to better string of the materials, the tool is somewhat angled from its vertical position.

There are many variations in the process of FSW that makes it difficult to conduct a thrill investigation. Major, independent variables are: rotational speed of the tool, tool advancing speed, magnitude of downward force to hold the touch between tool and piece steady, tool geometry, and tilt angle and type of material (thermophysical properties). These variables affect heat distribution as well as residual stress and
mechanical properties of the connection. A portion of the generated heat disseminated through work piece, will affect distortion, residual stress distribution as well as weld quality of the piece. Chao et al. [4] investigated the variations of heat energy and temperature produced by the FSW they point that only about 5% of the heat generated by the friction process flows to the tool and the rest flows to the work piece.

They formulated a boundary value problem for tool and workpiece in order to study the heat transfer in friction stir welding. They determined the frictional heat flux from the measured transient temperature fields obtained in the finite element analyses.

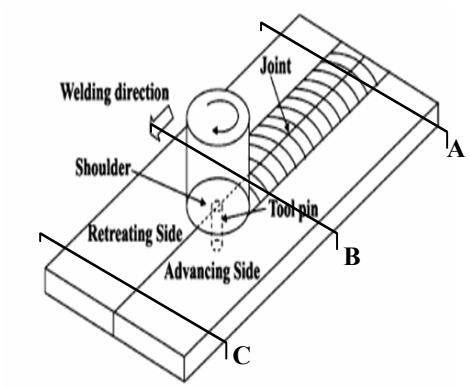

Fig. 1 Schematic illustrations of the friction stir welding process [3].

Schmidt et al. [5] proposed a general analytical model for heat generation based on two contact conditions at the tool/matrix interface, namely full sliding and full sticking condition. Mandal et al. [6] provided a theoretical framework for developing a thermo-mechanical hot channel approach for augmenting the FSW process. Song et al. [7] used a three dimensional heat transfer model to predict the temperature distributions in FSW. They assume that heat generated at the tool shoulder/work piece interface is frictional heat and the plastic strain is negligible. Zhang et al. [8–10] used the two- and three-dimensional thermo-mechanical model to analyze the material flows, temperature history and mechanical features in the FSW process. Nandan et al. [11, 12] have modeled a Three-dimensional visco-plastic flow of metals and the temperature fields in friction stir welding of 6061 aluminum alloy and 304L austenitic stainless steel.

Chen and Kovacevic [13] used a three-dimensional model based on finite element analysis to study the thermal history and thermo-mechanical process in the butt-welding of aluminum alloy 6061-T6. Their model was symmetry along the weld line and incorporated the mechanical reaction of the tool and thermo-mechanical process of the welded material [14, 15].

Peel et al. [16] reported the results of micro-structural, mechanical property, and residual stress investigations produced under varying conditions. They concluded that the weld properties were dominated by the thermal input rather than the mechanical deformation by the tool. Also, it was found out that the weld zone in FSW is in tension in both the longitudinal (parallel to tool travel) and transverse (perpendicular to tool travel) directions.

A simple three-dimensional thermomechanical model for friction stir welding (FSW) is presented. It is developed from the model proposed by Heurtier et al. (2006) [17] based on a combination of fluid mechanics numerical and analytical velocity fields. Mohamed assidi [18] used simplified numerical models and approaches the recent development of more accurate 3D simulation software which allows modeling the entire complexity of the FSW process , makes it possible to follow a much more rigorous inverse analysis (or calibration) approach ,FSW trials are conducted on an Al 6061 aluminum plate with an unthreaded concave tool. Force and tool temperature are accurately recorded at steady welding state for different welding speeds, the numerical simulations were based on an Arbitrary Lagrangian Eulerian (ALE) formulation that has been implemented in the Forge3 F.E. Software.Mohammad R. [19] investigated; three-dimensional numerical simulation of friction stir welding concerning the impact of tool moving speed in relation with heat distribution as well as residual stress.

Objective of this study was to predict numerical transient temperature distribution in Al7020-T53 plates that were welded by friction stir welding method for advancing speed of 40mm/min and rotational speed of 1400rpm. The model chosen for this task was the thermal model developed by Nandan [12] for FSW of aluminum alloy. The developed model was validating according experimental thermocouples data recorded; the thermal model was used to simulate the process. The model was then extrapolated to perform parametric studies in order to investigate effects of various process parameters on temperature distribution in the workpiece.

Model Description:

The welding process is shown in fig. (1) where travel speed is 40mm/min and rotational speed 1400rpm. The friction stir welding tool was fabricated from a tool steel labeled as X12M [20](density ρ=7800kg/m^3,specific heat C_p=500J/ kg.^{o}C and thermal conductivity k=40W/m.^{o}C) and is heat treatment includes heating the metal to 1020C^o for 30 min and then air cooling to room temperature. The tool had a concaved shoulder (2^o), while the cylindrical tool pin has a right hand threads of (1)mm pitch with a round bottom .the overall height of the pin is (4.7mm), made slightly shorter than the sheet thickness with shoulder diameter (18mm) and pin diameter (6mm) as shown fig.2.

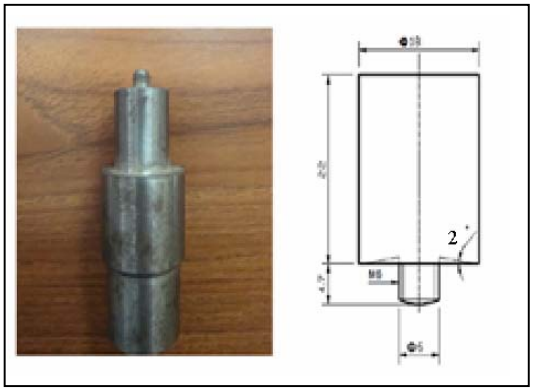

Fig. 2 the configuration of the tool used

The welded plate are AA 7020-T53 Al alloy, each is in rectangular shape with a size of (153*95*5 mm). The tool is considered a rigid solid, and the work piece is considered a ductile material characterized with elasticity, plasticity and kinetic hardening effect. The temperature-dependent properties of 7020-T53 Al alloy at various temperatures are given in table (1) [21], a piece of this alloy was analyzed to find its chemical composition by Spectro device in Specialized Institute for Engineering Industries (SIEI), table (2) shows the chemical composition.

The FSW process is divided into the following three phases: (a). the penetration phase, (b). the welding phase and (c). the tool pull-out phase. The heat is generated due to friction and plastic deformation at the tool and work piece interface during the process. During the welding period, the tool is moving at constant travel speed (40mm/min) and rotating speed (1400rpm) along the joint line.

Table 1: Thermal material properties of AA 7020-T53 Al alloy [21]

Temp.(k)	ρ(kg/m^3)	C_p (J/Kg k)	K(W/m.K)
300	2780	875	148
373	2770	910	159
473	2755	960	164
573	2740	980	173
673	2720	1040	182
733	2700	1100	196

Table (2) Chemical composition of AA 7020-T53

Si	Fe	Cu	Mn	Mg
0.166	0.256	0.142	0.111	1.29
Ni	Zn	Ti	Be	Pb
0.0037	4.61	0.0424	0.00062	0.0066
V	Zr	Al	Cr	Sn
0.0081	0.140	balance	0.213	≤0.0010

ANSYS® 12.0 was used for numerical simulation of friction stir welding process the thermal and mechanical responses of the material during friction stir welding process are investigated by finite element simulations. The finite element models are parametrically built using APDL (ANSYS Parametric Design Language) provided by ANSYS® [23]. Non-linearity of this model is because of the material nonlinearity.
Material nonlinearities occur because of the nonlinear relationship between stress and strain; that is, the stress is a nonlinear function of the strain. Non-linear relations appear because of temperature dependent mechanical properties [22].

Thermal Model:

The purpose of the thermal model is to calculate the transient temperature fields developed in the workpiece during friction stir welding.
In the thermal analysis, the transient temperature field T which is a function of time t and the spatial coordinates (x,y,z), is estimated by the three dimensional nonlinear heat transfer equation (1).

$$\left(\frac{\partial}{\partial}(k_x(T)(\frac{\partial T}{\partial x})+\frac{\partial}{\partial}(k_y(T)(\frac{\partial T}{\partial y})+\frac{\partial}{\partial}(k_z(T)(\frac{\partial T}{\partial z})\right)+$$

$$Q_{\text{int}}=\frac{\partial(c(T)\rho(T)T}{\partial t} \quad (1)$$

where k(T) is the coefficient of thermal conductivity , Q_{int} is the internal heat source rate, cp(T) is the mass-specific heat capacity, and ρ(T) is the density of the materials. The heat transfer model developed for the thermal analysis is described in the following section.

Assumptions: A number of assumptions have been made in developing the finite element thermal model, which includes:

- Workpiece material is isotropic and homogeneous.
- No melting occurs during the welding process.
- Thermal boundary conditions are symmetrical across the weld centerline.
- Heat transfer from the workpiece to the clamp is negligible.
- Two symmetry planes are applied on lateral sides of the workpiece.

Elements Used In the present thermal analysis, the workpiece is meshed using a brick element called SOLID70. The element is defined by eight nodes with temperature as single degree of freedom at each node and by the orthotropic material properties.

Boundary Condition
Boundary condition for FSW thermal model were specified as surface loads through ANSYS® codes. Assumptions were made for various boundary conditions based on data collected from various published research papers [24, 25]. Convective and radiative heat losses to the ambient occurs across all

free surfaces of the workpiece and conduction losses occur from the workpiece bottom surface to the backing plate. To consider convection and radiation on all workpiece surfaces except for the bottom, the heat loss q_s is calculated by:

$$q_s=\beta (T-T_o) + \varepsilon F\sigma(T^4-T_o^4) \quad (2)$$

where T is absolute temperature of the workpiece, T_o is the ambient temperature, β is the convection coefficient, ε is the emissivity of the plate surfaces, and σ= 5.67×10-8 W/m2 °K4is the Stefan-Boltzmann constant. In the current model, a typical value of was taken to be 30 /2K at ambient temperature of 300 K [30]and was taken to be (0.5) for aluminum alloy F is radiation view factors (F=1). In order to account for the conductive heat loss through the bottom surface of weld plates, a high overall heat transfer coefficient has been assumed. This assumption is based on the previous studies [4, 26]. The heat loss was modeled approximately by using heat flux loss by convection q_b given by ;

$$q_b=\beta_b (T-T_o) \quad (3)$$

where β_b is a fictitious convection coefficient. Due to the complexity involved in estimating the contact condition between the welded plate and the backing plate, the value of β_b had to be estimated by assuming different values through reverse analysis approach. In this study, the optimized value of β_b was found to be (100-300) w/cm^2℃.

The heat transfer coefficient at the bottom face depends on the local temperature and is given by following relation [31]:

$$\beta_b = \beta_{bo}(T - T_o)^{0.25} \quad (4)$$

Where β_{bo} is the heat transfer parameter for the bottom surface.

Figure (3) shows the schematic representation of boundary conditions that were used for thermal analysis.

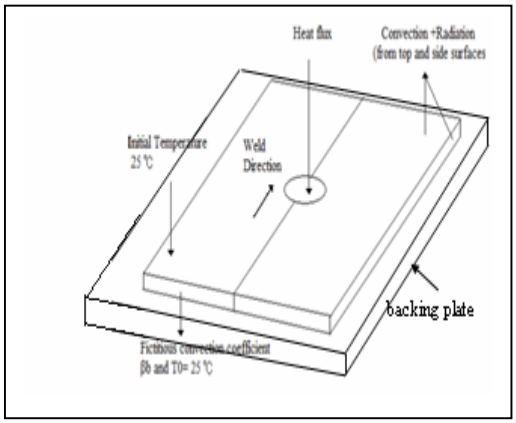

Fig. 3 Schematic representation of boundary condition for thermal analysis

Heat generation during friction-stir welding arises from two main sources: deformation of the material around the tool pin and the friction at the surface of the tool shoulder. A major difficulty is determining suitable values for the friction coefficient. The conditions under the tool are both extreme and very difficult to measure. To date, these parameters have been used as 'fitting parameters' where the model works back from measured thermal data to obtain a reasonable simulated thermal field. While this approach is useful for creating process models to predict, for example, residual stresses it is less useful for providing insights into the process itself. Mathematical approximations for the total heat generated by the tool shoulder may be used to compensate for deformation heat generation; this could be done by an adjusting coefficient of friction. Friction is a complex physical phenomenon that depends on parameters like material, surface roughness, lubrication, temperature and pressure. The effects of friction in metal forming simulations are commonly accounted for by Coulomb friction models [27]. Assuming slipping conditions, the friction coefficient is adjusted in order to calibrate the model. A wide range of published values for friction coefficient is within 0.3-0.85 [28], which reflect the experimental conditions.
Total frictional heat of shoulder at rubbing angular speed of$(1-\delta)\omega$, will be:

$$Q_s = \frac{2}{3}\pi(1-\delta)\omega\mu PR_s \quad (5)$$

where Q_s heat generation by shoulder, ω rotational speed rps, μ coefficient of friction, P pressure , R_s radius of shoulder and δ is the slip factor that

compensate for tool/material relative velocity. Typical values for slip factor found in literature ranges between 0.6, 0.85 [29].

In similar concept, heat generated by lateral surface of the pin is:

$$Q_p = 2\pi(1-\delta)\,\omega\,\mu\,P L_p\,R_p^2 \qquad (6)$$

where Q_p heat generation by pin surface, ω rotational speed rps , μ friction coefficient, P axial pressure N/m2, L_p pin length and R_p pin radius

Total frictional heat generated by the tool is the summation of equations (5) and (6) which is:

$$Q_T = 2\pi(1-\delta)\omega\mu P\left((R_s^3/3) + L_p\,R_p^2\right) \qquad (7)$$

During the process the tool travels at a constant speed (V_t). This motion was simulated by changing heat source location, as shown in figure (4), according to the following equation:

$X_{i+1} = X_i + V_t\,\Delta t$ for $L_i \le X \le L_w$

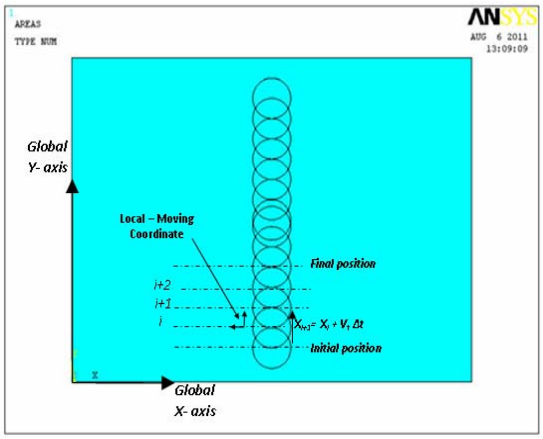

Fig. 4 Modeling of Heat Source Movement at Different Time Steps.

Where Δt is the time required for the tool to travel from location X_i to X_{i+1}, (i.e. element size) and V_t is the tool traveling speed.

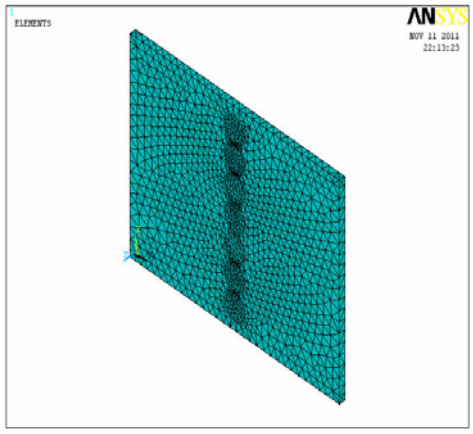

Fig. 5 Finite Element Model and Mesh.

The finite element equation after applying boundary condition can be expressed in matrix form[;

$$T^e(x,y,z,t) = [N(x,y,z,t)]\{T^e\} \qquad (8)$$

$$[N(x,y,z)] = [N_i(x,y,z)\quad N_j(x,y,z)\ N_p(x,y,z)\ ] \qquad (9)$$

$$\{T^e\} = \begin{Bmatrix} T_i(t) \\ T_j(t) \\ Tp(t) \end{Bmatrix} \qquad (10)$$

$$\frac{\partial T^e}{\partial x} = \left[\frac{\partial N_i}{\partial x}\frac{\partial N_j}{\partial x}\frac{\partial N_p}{\partial x}\right]\{T^e\} \qquad (11)$$

$$\frac{\partial}{\partial T_m}\left(\frac{\partial T^e}{\partial x}\right) = \frac{\partial N_m}{\partial x} \qquad (12)$$

$$\frac{\partial T^e}{\partial T_m} = N_m \qquad (13)$$

$$\frac{\partial T^e}{\partial t} = [N]\{\dot{T}\} \qquad (14)$$

Where

$$\left\{\dot{T}^e\right\} = \begin{Bmatrix} \frac{\partial T_i}{\partial t} \\ \frac{\partial T_j}{\partial t} \\ \frac{\partial \dot{T}_p}{\partial t} \end{Bmatrix} \qquad (15)$$

$$[k]\{T\}+[\dot{k}]\left\{\dot{T}\right\}=\{F\} \quad (16)$$

Where

$$[k]=\sum_{e=1}^{ne}\left[[k_1{}^e]+[k_2{}^e]\right] \quad (20)$$

$$\left[\dot{k}\right]=\sum_{e=1}^{ne}\left[k_3{}^e\right] \quad (21)$$

And

$$\{F\}=\sum_{e=1}^{ne}\{F^e\} \quad (22)$$

The expression for K_1, K_2, K_3 and F can be stated using matrix notation

$$[K_1]=\iiint_v [B]^T[D][B]dv \quad (23)$$

$$[K_2]=\iiint_s h[N]^T[N]dS \quad (24)$$

$$[K_3]=\iiint_v \rho c[N]^T[N]dv \quad (25)$$

$$\{F^e\}=\int_{ve} Q[N]^T dv+\int_{s_2e} hT_\infty[N]^T ds_2-\int_{s_3e} q[N]^T ds_3 \quad (26)$$

$$D=\begin{bmatrix}K_x & 0 & 0\\ 0 & K_y & 0\\ 0 & 0 & K_z\end{bmatrix} \quad (27)$$

$$[B]=\begin{bmatrix}\frac{\partial N_1}{\partial x} & \frac{\partial N_2}{\partial x} & \frac{\partial N_3}{\partial x} & \cdots & \frac{\partial N_8}{\partial x}\\ \frac{\partial N_1}{\partial y} & \frac{\partial N_2}{\partial y} & \frac{\partial N_3}{\partial y} & \cdots & \frac{\partial N_8}{\partial y}\\ \frac{\partial N_1}{\partial z} & \frac{\partial N_2}{\partial z} & \frac{\partial N_3}{\partial z} & \cdots & \frac{\partial N_8}{\partial z}\end{bmatrix} \quad (28)$$

N_1, N_2, N_3….. N_8 are shape functions is natural coordinate system for brick element.

$$N_i=\frac{(1+\xi\xi_i)(1+\eta\eta_i)(1+\zeta\zeta_i)}{8} \quad (29)$$

With $\xi_i, \eta_i, \zeta_i = \pm 1$ and i=1,2,3…..8

Simulation

The thermal modeling was carried out in transient thermal analysis. Its main features are an Arbitrary Lagrangian Eulerian (ALE) formulation. To build the model a title was specified for the analysis and preferences were set for the options to display (thermal). Then ANSYS preprocessor (PREP7) was used to do these tasks:

- Define element types and options.
- Define material properties.
- Create model geometry.
- Mesh the model geometry.

The transient analysis was managed either by defining multiple load steps (for stepped or ramped boundary conditions) or by using a single load step and tabular boundary conditions (for arbitrary time-varying conditions) with an array parameter to define the time points. To use the load step method, this procedure was followed:

- Specify the time at the end of the load step.
- Specify whether the loads are step or ramp.
- Specify the load values at the end of the load step.
- Write information to a load step file.
- Repeat these steps for the next load step, and so on until finishing all load step data.
- Since the problem involves nonlinear analysis, full Newton-Raphson option was used to solve the nonlinear equations.

Force and temperature measurements:

Experiments are conduct under different welding rotational ,four cases are considered with differing tool rotational speeds (710rpm,900rpm,1120rpm and 1400rpm) a component dynamometer based on load cell (SEWHA,2000kg capacity, R.O:2.0008mV/V) is used for measuring the vertical force during the FSW process for penetration time 60sec after that tool is moved with constant travel speed. This load cell for vertical force measurement is fixed on the rotating tool, and transmitter is used for transmitting the analog force data to the weight indicator capacity (2000kg) (SEWHA, SI4010) fig. (6) and fig. (7) Show the vertical force measured from FSW process for different tool rotational speed. The sampling frequency of data for force measurement is 10Hz.

Fig.6 Vertical load cell measuring sensors.

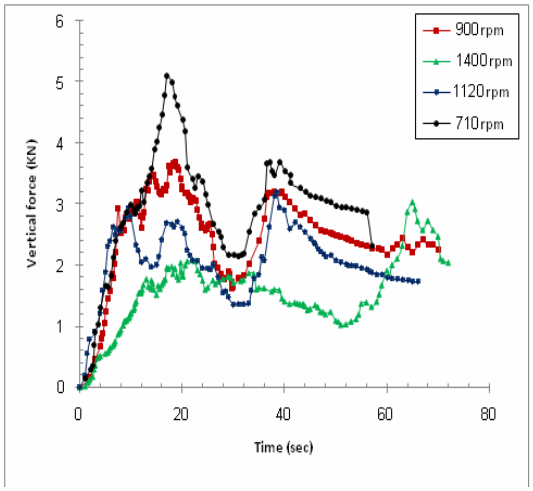

Fig. 7 Vertical force penetration of tool on the workpiece during the FSW process.

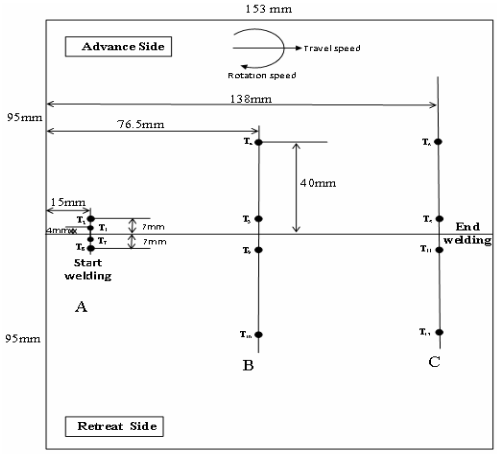

Fig. 8 thermocouple positions on the workpiece

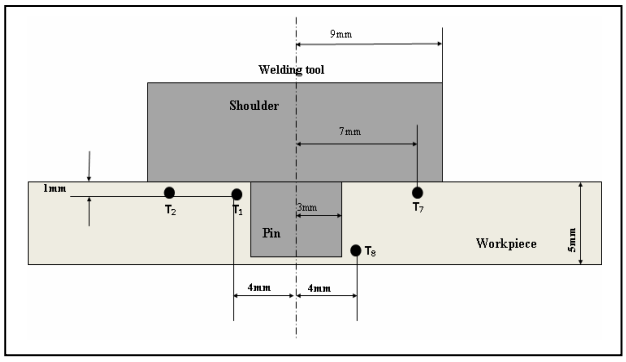

Fig. 9 Thermocouples position at tool penetration on workpiece at section A-A.

Fig. 10 Temperature recorder and hole drill thermocouple position on workpiece.

the plates are prepared to measure the temperature at (12 locations using k type thermocouples at three sections (A, B and C) as shown in fig.(1) calibrated in central organization for standardizon quality control, The locations of thermocouples in the workpiece are shown in fig.(8). Thermocouples connected to the 12 channels reader, Transient temperatures are recorded in the 12channels during FSW process; thermocouples are attached to SD card data logger temperature recorder (BTM-4208SD), range (-100 to 1100 ^{o}C).

For section (A) in fig. (8), four thermocouples (channels 1, 2, 7 and 8) are located in heat affected zone (HAZ) for (channels 2 and 7 in advance and retreat side respectively) and the other thermocouples (channels are located in nugget zone NZ) as shown in fig. (9).

Results and discussion:

During the penetration phase, the rotating tool pin penetrates into the workpiece until the tool shoulder comes in contact with the workpiece. The penetration speed is chosen to be (0.0783mm/sec) in the model, and the corresponding penetration time is approximately (80sec).

convection heat transfer coefficient with backing plate ($300W/m^2k$) , convection heat transfer coefficient($30W/m^2k$), ambient and initial temperature (T_o=293K), slip factor (δ=0.6), friction coefficient (μ=0.41), (axial load=2kN) , Heat generation(Q=331watt) used as input welding parameters in the finite element calculation with their corresponding vertical force in the workpiece predicted in fig.(7) the plasticization of material under the tool increases with increasing rotational speed and with decrease in tool traverse speed resulting the reduction of vertical force.

The finite element simulation couples the moving tool with the workpiece and also considers the thermal effect of the initial tool pin penetration before start of the weld

Fig. (11) Present cross-sectional views of the calculated temperature contours in the workpiece and tool at different time during the penetration. This figure graphically illustrates the temperature history of the workpiece and the tool during the pin penetration. The highest temperature is observed in the centre of the weld region extending down from the crown surface to the probe root side, since the rotation of the shoulder and the probe (pin) contributes the highest heat flux in this region. The relatively higher heat dissipation through the contact surface between the welded plate and the backing plate as compared with the top surface the top surface of the plate causes the temperature contour in the weld nugget area the follow a "V" shape .This is because of the relatively higher convection coefficient at the bottom surface of plate as compared with the top surface. It is believed that the described "V" –type distribution of the temperature in the weld zone contributes to the grain coarsening in the TMAZ and the HAZ.

Fig. (12) and fig. (13) show the experimentally thermocouples reading and FEM result for (channel T1) that located 4.5mm from joint line and at (channel T8) located 1mm in the bottom of workpiece as shown in fig.(9).

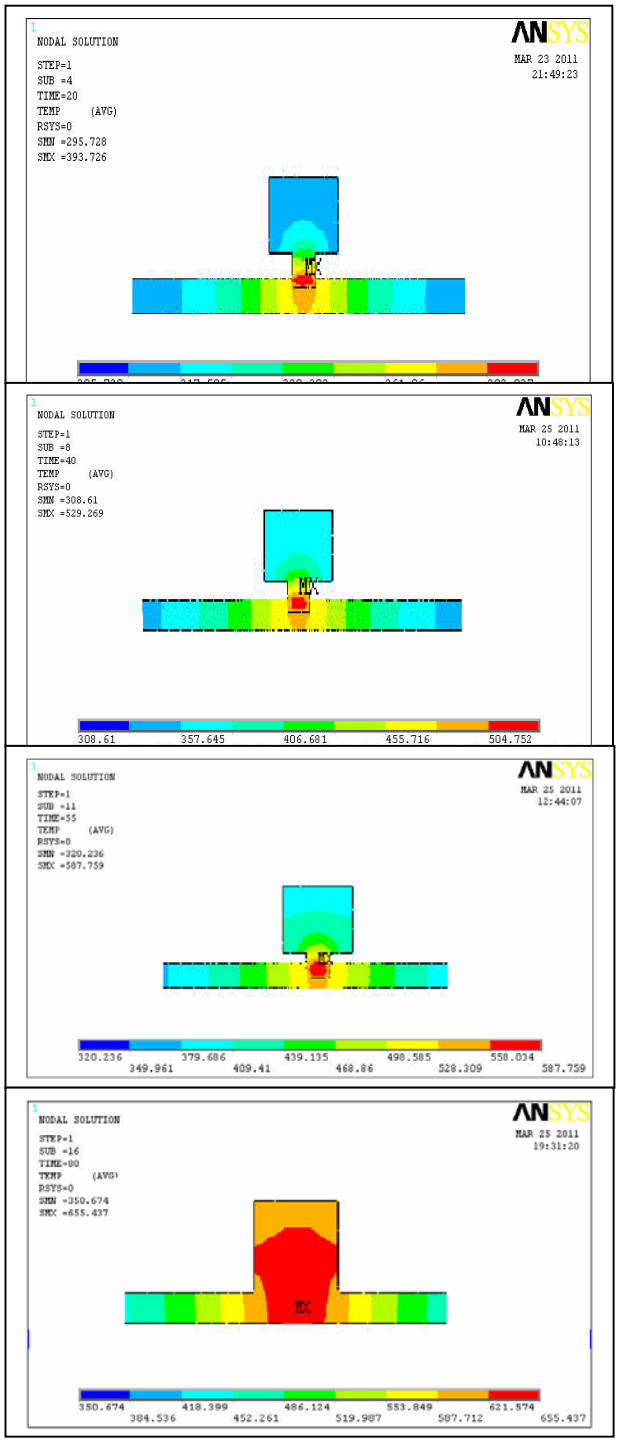

Fig. 11 Temperature-Time history for tool and workpiece during tool pin penetration (V_t=40mm/min,ω=1400rpm)

Fig. (14) shows the effect of thermocouple position where (T1) at the top and (T8) at the bottom, (T1; 645 ^{o}K) is higher than (T8; 635.79^{o}K), initially T1 increase with pin penetrate in the work piece while the pin continue of penetrate action T8 sense increasing in temperature but T1 still higher than T8 due to contact of shoulder which increased the temperature that increase by stirring and friction around the pin.

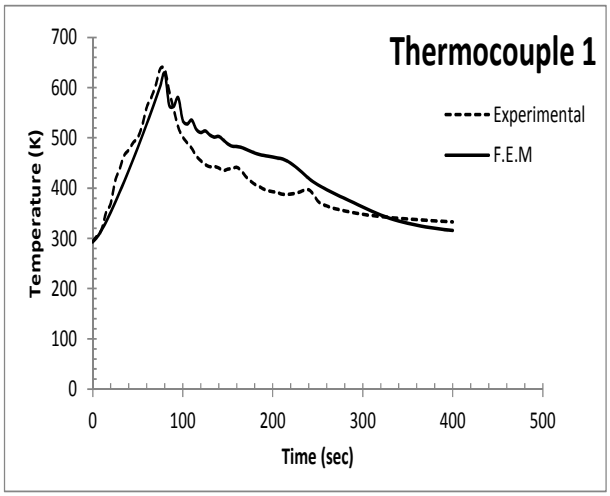

Fig. 12 Comparison of the modeled and measured temperature history for thermocouple T1

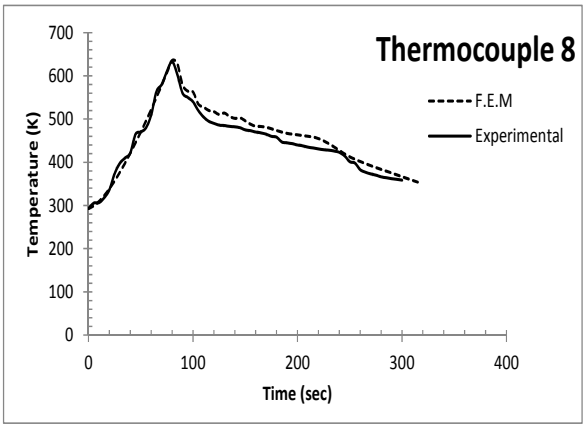

Fig. 13 Comparison of the modeled and measured temperature history for thermocouple T8

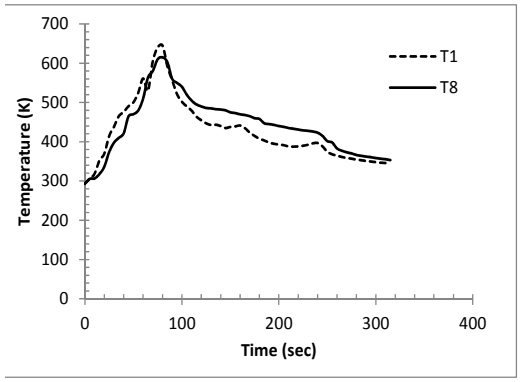

Fig. 14 Comparison measured temperature history for thermocouple location 4mm from joint line at top (T1) and bottom (T8)

Fig.15; shows temperature recorded by thermocouple T2(629K) in advance side at location 7mm from joint centre line fig.(9), in retreate side thermocouple T7(605K) at location 7mm from joint centre line fig.(9). Experimentally result shows the temperature in advance side is higher than retreate side because material flow and plastic deformation around tool moving from advance side to retreate side additional to friction heat under the shoulder that gives higher temperature the computational results show that the material flows on the retreating and the front sides are higher. So, the slipping rates on the retreating and the front sides are lower than the ones on the trailing and advancing sides. This is the reason that the heat fluxes on the trailing and the advancing sides are higher, which leads to the fact that the temperatures are higher in this region for both thin plates [32].

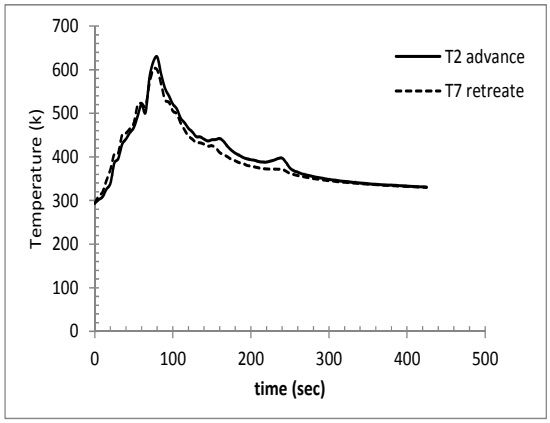

Fig. 15 shows thermocouples measured value in advance T1 and retreate side T7 at section A-A

Fig.16 shows the maximum temperature while the tool ending the penetration (80sec) ,shoulder is in contact with the surface of workpiece so that in section A-A thermocouple T1 in advance side at location 4mm from joint centre line recorded maximum temperature (645K), thermocouple T2 in advance side at location 4mm from joint centre line recorded maximum temperature (637K) and thermocouple T7 in advance side at location 4mm from joint centre line recorded maximum temperature (605K) it noticeable that temperature difference along two sides (advance and retreate) of welding centre line, but in simulation the temperature is symmetric along welding centre line at each side [31] .

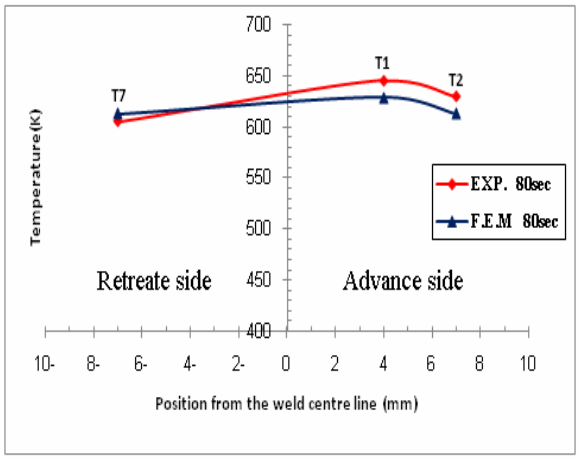

Fig. 16 comparison of simulated and measured temperature along transverse direction at section A-A (end of penetration)

Fig. (17); shows numerical simulation of the temperature history at 7mm along welding line in advance side where (TEMP-2) at section A-A with time 80sec welding tool ending penetration phase (dwell), (TEMP-3) at section B-B with time 160sec welding tool at mid position of welding line and (TEMP-5) at section C-C with time 240sec welding tool pullout at end of welding line.

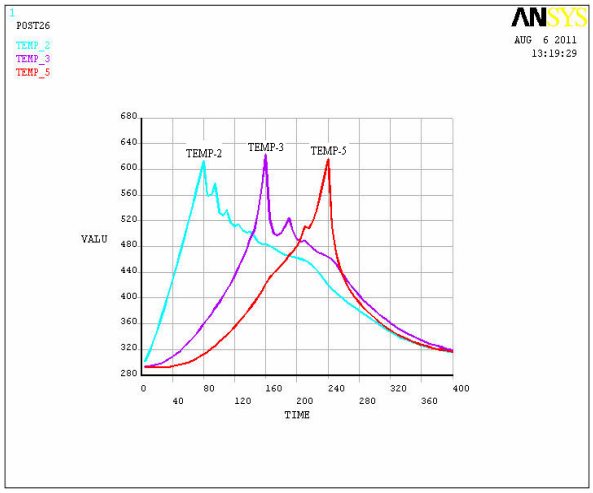

Fig.(17) Temperature-time profile for F.E.M value at location 7mm from joint line in advance side (V_t=40mm/min, ω=1400rpm)

Fig. (18) Shows a comparison of experimental value and F.E modeled value for thermocouple T3 at section B-B while the tool traveled at mid position along tool movement in welding line at time 160sec.

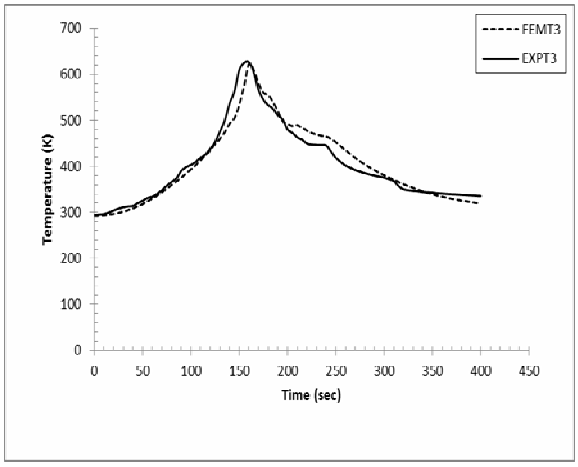

Fig. 18 Comparison of the modeled and measured temperature history for thermocouple T3 location 7mm from joint line on advance side in section B-B

Fig. (19) Shows comparison of experimental value and F.E modeled value for thermocouple T5 in section C-C while the tool traveled at end welding line at time 240sec.

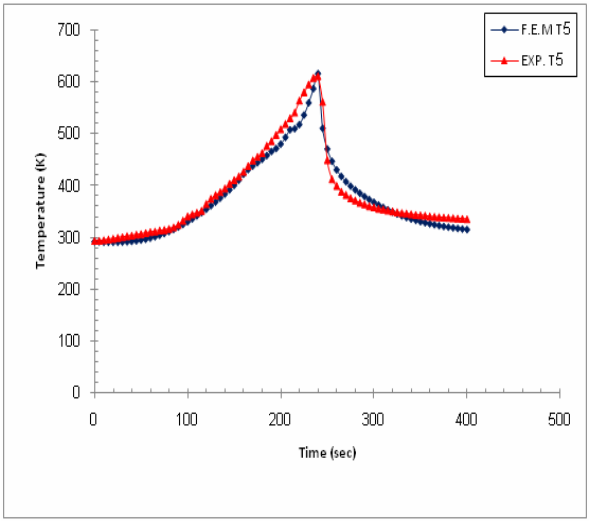

Fig. 19 Comparison of the modeled and measured temperature history for thermocouple T5 location 7mm from joint line on advance side in section C-C.

Fig. (20) shows modeling temperature contour distribution when the tool moving along welding line at mid position of the workpiece at time 160sec ,the temperature distribution effected by heat conduction between the work piece with fixture and by convection, radiation ambient travel speed also has influence on temperature distributions travel speed and rotating speed on transient temperature distribution.

Fig. (21) shows finite element modeling of the distribution of temperature in the transverse direction of welding line in the section B-B when welding tool at mid position of workpiece and according to assumption symmetric value in advance and retreate side T_{max}=642K for (1400rpm-40mm/min.

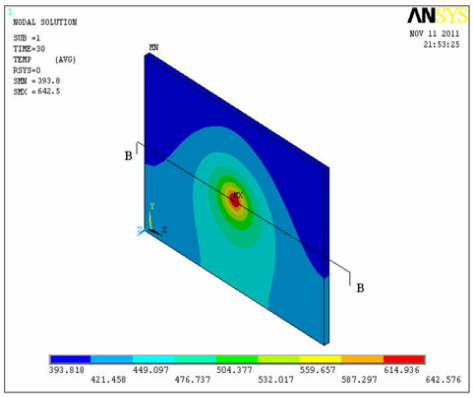

Fig. 20 temperature gradient contour in the top surface of the workpiece at the movement the tool moves to the middle point of the plate (ω=1400rpm and V_t=40

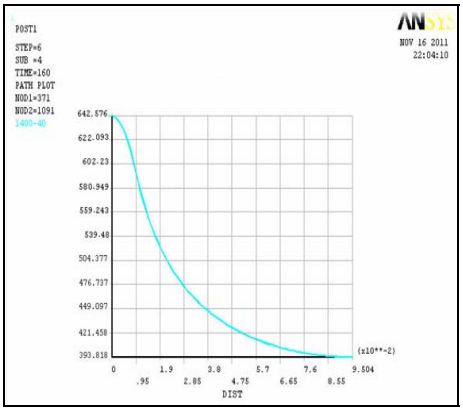

Fig. 21 Finite element temperature distribution in mid position in work piece sec B-B in direction perpendicular to welding line at welding parameter (ω=1400rpm and

Fig. (22) shows temperature modeled and measured at section B-B when tool position at mid welding line with time 160sec, thermocouples T3, T4 in

advance side and T9, T10 in retreate side (the letter T refer to thermocouple number and position), the thermocouples placed at depths 0.5mm below the top surface thermocouple reading shows temperature in advance (T3=626.6K) is larger than retreate side (T9=609.1K).

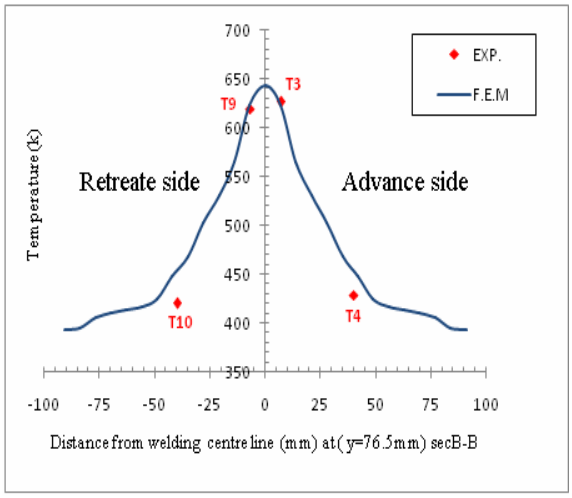

Fig. 22 comparison of F.E.M value and measured temperature distribution of along transverse direction welding line at sec.B-B (ω=1400rpm and V_t=40 mm/min).

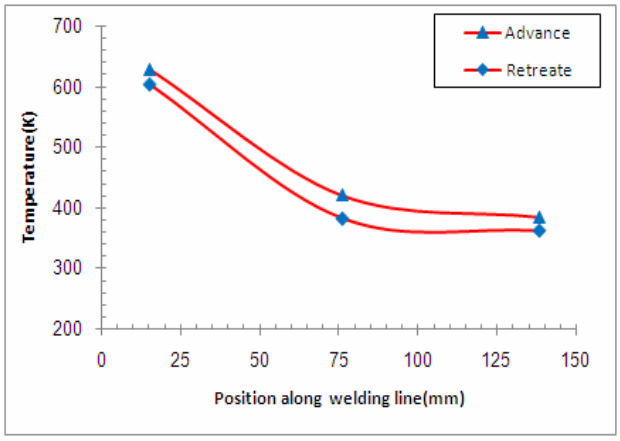

Fig.23 Measured temperature along welding line at starting tool moving (80sec) (V_t=40mm/min, ω=1400rpm)

Fig. (23), fig.(24) and fig.(25) show thermocouples measured temperature when tool moving along welding line at three position start, mid and end moving figures show the difference reading between advance side and retreating side.

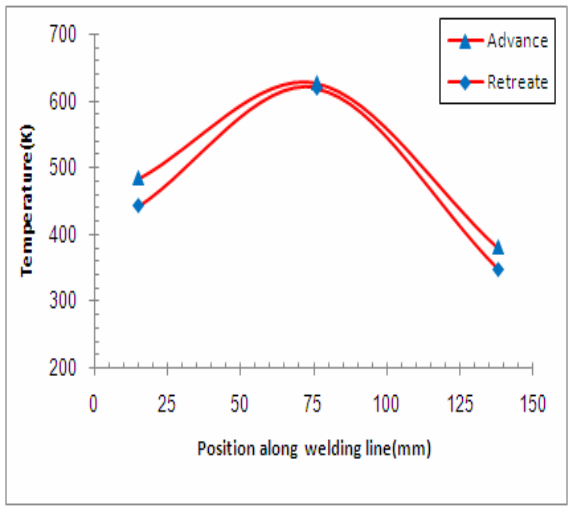

Fig. 24 Measured temperature along welding line at mid tool moving (160sec) (V_t=40mm/min, ω=1400rpm)

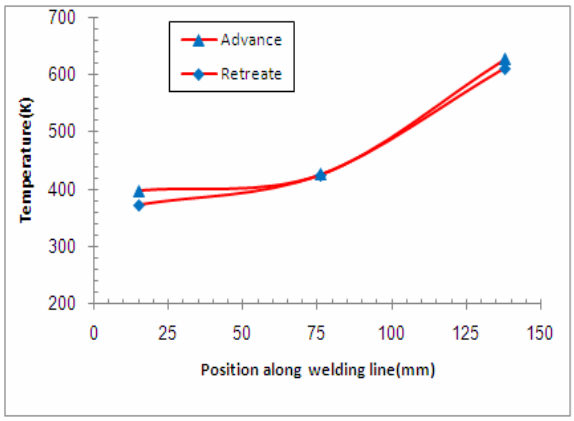

Fig. 25 Measured temperature along welding line at end tool moving (240sec) (V_t=40mm/min, ω=1400rpm)

Fig.26 and fig.27 shows temperature contours when penetration of welding tool in the workpiece, temperature increases with increase tool penetration with two stages: first stage when tool pin penetrate into the workpiece when the tool moving axially with constant axial speed and second stage when tool shoulder contact with workpiece in this time end dwell and then the welding tool moving at constant travel speed 40mm/min. A figure shows that the maximum temperature gradient happens in the region formed by the edge of the shoulder. This event is attributed to the fact that the highest heat generation in this region and the highest heat

radiation and convection dissipations of the region occur just beyond the shoulder edge [25].

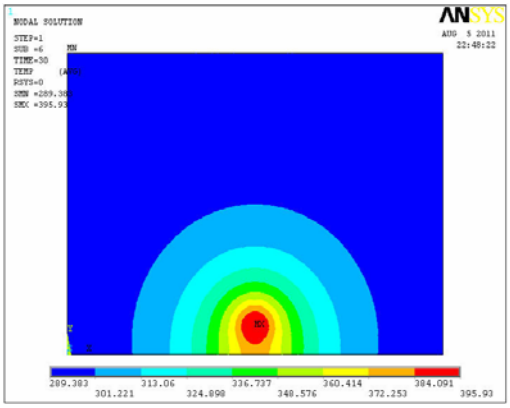

Fig.26 Temperature Distribution at time 30 sec (Dwell)

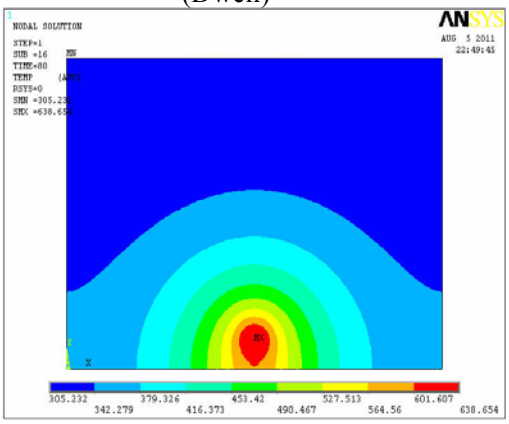

Fig.27 Temperature Distribution at time 80 sec (end of Dwell)

Fig.28 to fig.32 shows thermal distribution when the tool penetrates in workpiece (beginning the welding process) at time 80sec, then start moving of the tool along welding line to mid position of the workpiece at time 160sec and the end position of welding tool at time 240sec after that welding tool pullout from workpiece and then work piece cooled as shown in

fig.31. The temperature distribution effected by heat conduction between the work piece with fixture and by convection, radiation ambient travel speed also has influence on temperature distributions increase travel speed decrease temperature history [25].

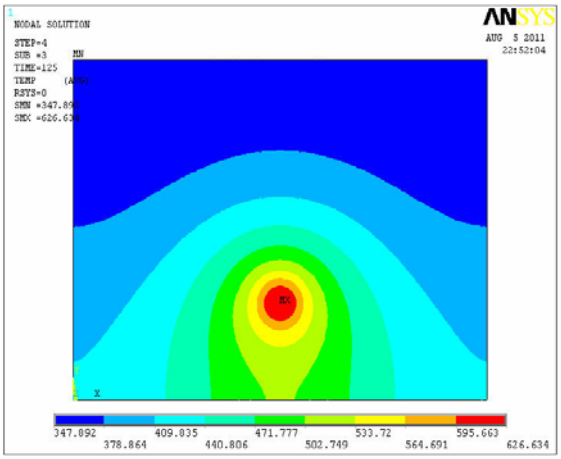

Fig.28 Temperature Distribution at time 125 sec (welding tool moving along welding line)

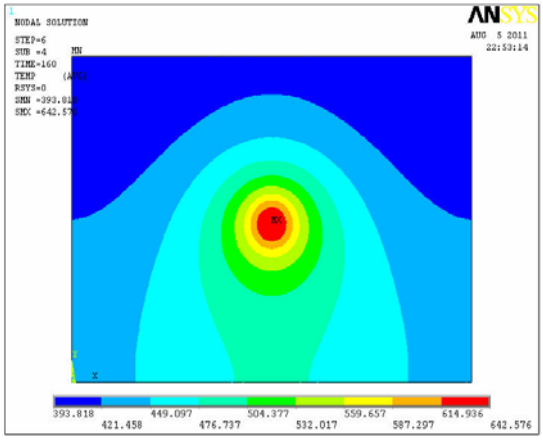

Fig.29 Temperature Distribution at time 160 sec moving welding tool at mid position of welding line

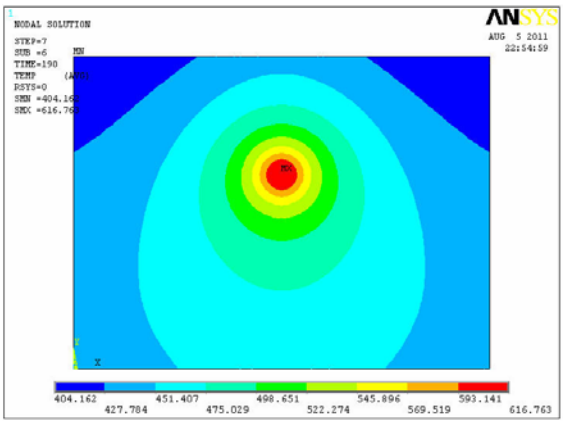

Fig.30 Temperature Distribution at time 190 sec (welding tool moving along welding line)

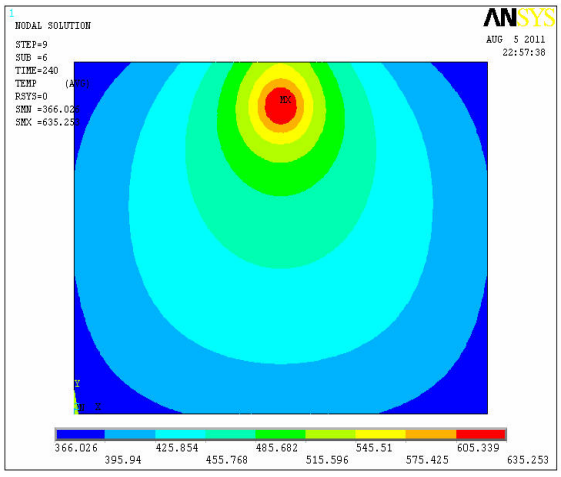

Fig.31 Temperature Distribution at time 240 sec (End of Moving) tool pullout

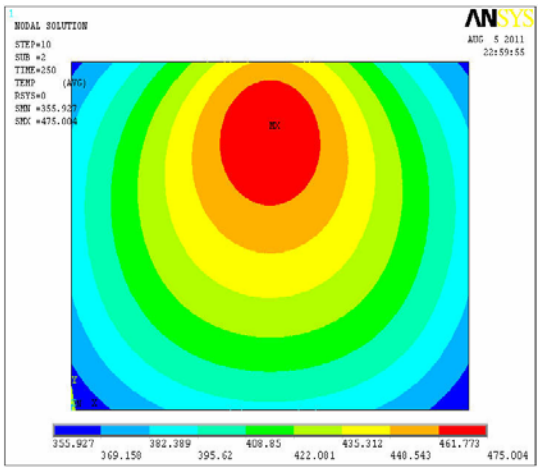

Fig.32 Temperature Distribution at time 250 sec (Cooling)

Conclusion:

To study the variations of transient temperature in friction stir welding of AA 7020-T53 plates, detailed three-dimensional nonlinear thermal simulations are performed for the FSW process using the finite element analysis ANSYS. 40 mm/min travel speed with tool rotational speeds of 1400 rpm is considered. From the analyses, we can summarize the results as follows:

- Axial load measured from experimental work decreases with increasing rotational speed because that decrease in strength due to temperature increases in penetration position.
- The experimental data show the maximum temperature measured during FSW at mid position 629k and numerically value from the simulation is 642k^{o}, which is significantly less than the melting temperature of 7020-T53 aluminum alloy at 916K^{o}.
- The temperature measured at advance side (629k) is higher than retreate side (605k).
- Numerical results (Tmax =642K) agreement with measured data (Tmax=629k) (error 2%).
- The computational results show that the material flows on the retreating and the front sides are higher. So, the slipping rates on the retreating and the front sides are lower than the ones on the trailing and advancing sides. This is the reason that the heat fluxes on the trailing and the advancing sides are higher, which leads to the fact that the temperatures are higher in this region for both thin plates.

Reference:

1. Zhang Z; Zhang HW (2008) "A fully Coupled Thermo-Mechanical Model Of Friction Stir Welding". Int. J. Adv. Manuf. Technol. 37:279–293.
2. Cho JH, Boyce DE, Dawson PR. (2005)."Modeling Strain Hardening and Texture Evolution in Friction Stir Welding of Stainless Steel". Mater. Sci. Eng. 398:146–163.
3. Nandan R. DebRoy T. Bhadeshia HKDH (2008). "Recent Advances in Friction-Atir Welding Process, Weldment Structure and Properties". Prog. Mater. Sci. 53:980–1023.
4. Chao YJ. Qi X. Tang W. (2003) "Heat transfer in Friction Stir Welding Experimental and Numerical Studies". J. Manuf. Sci. Eng. 125:138–145.
5. Schmidt HB. Hattel JH. (2008)." Thermal Modeling of Friction Stir Welding". Scr. Mater. 58:332–337.
6. Mandal S, Williamson K (2006)." A thermo-Mechanical Hot Channel Approach For Friction Stir Welding". J. Mater. Process. Technol. 174:190–194.
7. Song M. Kovacevic R. (2003)." Thermal Modelings of Friction Stir Welding in A moving Coordinate System and Its Validation". Int. J. Mach. Tools. Manuf. 43:605–615.
8. Zhang HW. Zhang Z. Chen JT. (2005)." The finite Element Simulations of The friction Stir Welding Process". Mater. Sci. Eng. 403:340–348.
9. Zhang Z. Zhang HW. (2007)." Material behaviors and Mechanical Features in Friction Stir Welding Process". Int. J. Adv. Manuf. Technol. 35:86–100.
10. Zhang Z. Zhang HW. (2009)." Numerical studies on Controlling of Process Parameters in Friction Stir Welding". J. Mater. Process.Technol. 209:241–270.
11. Nandan R. Roy GG. Debroy T. (2006)." Numerical Simulation of Three-dimensional Heat Transfer and Plastic Flow During Friction Stir Welding". Metall. Mater. Trans. 37A:1247–1259.
12. Nandan R. Roy GG. Lienert TJ. Debroy T. (2006)." Numerical Modeling of 3D plastic flow and Heat Transfer During Friction Stir Welding of Stainless Steel". Sci. Technol. Weld. Joining 11:526–537.
13. Chen CM. Kovacevic R. (2003)." Finite Element Modeling of Friction Stir Welding Thermal and Thermomechanical Analysis". Int. J. Mach. Tools Manuf. 43:1319–1326.
14. Buffa G, Hua J, Shivpuri R, Fratini L (2006)." A Continuum Based FEM Model for Friction Stir Welding Model Development". Mater. Sci Eng 419:389–396.
15. Rajesh SR. Bang HS. Chang WS. Kim HJ. Bang HS. Oh CI. Chu. JS. (2007)." Numerical Determination of Residual Stress in Friction Stir Weld Using 3D-analytical Model of Stir Zone". J. Mater. Process. Technol. 187–188:224–226.
16. Peel M. Steuwer A. Preuss M. Withers. PJ. (2003) "Microstructure, Mechanical Properties and Residual Stresses as A function of Welding Speed in Aluminum AA5083 Friction Stir Welds". Acta. Mater. 51:4791–4801.
17. Heurtier et al., 2006 P. Heurtier, M.J. Jones, C. Desrayaud, F. Montheillet, D. Allehaux and J. Driver, (2006) "Mechanical and thermal modeling of friction stir welding", J. Mater. Process. Technol. 172, pp. 152–158.1
18. Mohamed Assidi, Lionel Fourment, Simon Guerdoux, Tracy Nelson (2010)" Friction Model for Friction Stir Welding Process Simulation: Calibration From Welding Experiments" International Journal of Machine Tool Manufacture (50) 143-155.
19. Mohammad R. & Hamidreza N. (2011) "Analysis of Transient Temperature and Residual Thermal Stresses in Friction Stir Welding of Aluminum Alloy 6061-T6 Via Numerical Simulation" Int. J. Adv. Manuf. Technol. 55:143–152.
20. Key to steel data base version (2007.5).
21."Properties and Selection: Non-Ferrous Alloys and Special Purposes Materials", ASM Handbook, American Society for Metals, Vol. 2, 1992.
22. Manthan Malde (2009)" Thermomechanical Modeling and Optimization of Friction Stir Welding" MS.c Thesis, Osmania University, Hyderabad, India.
23. ANSYS® Release 12.0 Documentation, ANSYS Inc, 2009.
24. Yousif, Mohanned Akab, (2006) "Investigation of Mechanical and Microstructural Characteristic of Friction Stir Welded Joints." Ph.D. Thesis, University of Baghdad.
25. Muhsin Jabir Jweeg ,Sarmad Dhia Ridha (2010) "An investigation of friction stir welding and stress relief by vibration of 6061-T6 aluminum alloy" Ph.D. Thesis, University of Baghdad.
26. Zhu, X.K. and Chao, Y.J., (2004) "Numerical Simulation of Transient Temperature and Residual Stresses in Friction Stir Welding of 304L Stainless Steel", Journal of Materials Processing Technology,. 146(2): p. 263-272.
28. Hansson, Sofia, "Simulation of Stainless Steel Tube Extrusion" Luleå University of Technology,

Sweden, 2006.
28. Dixon, John, Burkes, Douglas and Medvedev, Pavel, (2007) "Thermal Modeling of A Friction Bonding Process" Proceedings of the COMSOL Conference ,Boston,.
29. Seidel, T.U. and Reynolds, A.P. (2001) "Visualization of the Material Flow in AA2195 Friction-Stir Welds Using a Marker Insert Technique." Metallurgical and Materials Transactions A, Vol. 32A, pp 2879-2884.
30. Nandan, R., Roy, G.G., and Debroy, T., (2006) "Numerical Simulation of Three-Dimensional Heat Transfer and Plastic Flow during Friction Stir Welding." Metallurgical and Materials Transactions A Vol. 37A, pp 1247-1269.
31. A. Arora, R. Nandan, A.P. Reynolds and T. Debroy. (2009)" Torque, power requirement and stir zone geometry in friction stir welding through modeling and experiments" Scripta Materialia (60) 13-16.
32. H. Jamshidi Aval & S. Serajzadeh & A. H. Kokabi (2011) "Theoretical and experimental investigation into friction stir welding of AA 5086 "Int. J. Adv. Manuf. Technol. 52:531–544.

Nomenclature

ρ Density (kg/ m^3)
cp Specific heat capacity (J/ kg°k)
k Thermal conductivity (w /m°k)
T Temperature (°k)
T_o Ambient temperature (°k)
ε emissivity
σ Stefan –Boltzmann (w/m^2 $^o k^4$)
μ Friction coefficient
P Contact pressure (N/ m^2)
ω rotation speed (rpm)
V_t travel speed (mm/min)
δ Slip factor
R_s shoulder radius (mm)
R_p pin radius (mm)
L_p pin length (mm)
Q_s Friction heat shoulder (w)
Q_p Friction heat pin (w)
Q_T Total heat generation (w)
i Time step
t Time (s)
Δt Time change (s)
Q_{int} Heat generation (w/ m^3)

F radiative view factor
β convection coefficient
β_b fictitious convection coefficient
β_{bo} is the heat transfer parameter for the bottom surface